Binary Actuation of Solar Mirrors

by

Teresa M. Gomez

Submitted to the Department of Mechanical Engineering
in partial fulfillment of the requirements for the degree of

Bachelor of Science in Engineering
as recommended by the Department of Mechanical Engineering

at the

Massachusetts Institute of Technology

June 2011

Signature of Author . . . . . .
Department of Mechanical Engineering
May 5, 2011

Certified by . . . . . .
Steven Dubowsky
Professor of Mechanical Engineering
Thesis Supervisor

Accepted by . . . . . .
John H. Lienhard V
Collins Professor of Mechanical Engineering
Chairman, Undergraduate Thesis Committee

Binary Actuation of Solar Mirrors

by

Teresa M. Gomez

Submitted to the Department of Mechanical Engineering
on May 5, 2011 in Partial Fulfillment of the Requirements
for the Degree of Bachelor of Science in Engineering
as Recommended by the Department of Mechanical Engineering

Abstract

This thesis explores the use of binary actuators to adjust the shape of an array of mirrors. To explore this concept, an experimental system was refurbished and recalibrated. This experimental system was used to explore the range of possible configurations that could be reached by a simple binary actuated system.

System models are required for accurate control of these binary actuated structures. This thesis develops and tests the accuracy of two different modeling approaches, linear and iterative. The linear model assumes that each actuator contributes a constant value to the angle of the center mirror, and that this value is not dependent on the other actuator positions. The actuator contributions are summed to find the angle of the center mirror. These contributions are found two ways: by taking a relevant single data point for each actuator, and by using a least squares fitting of a large subset of data. The iterative model assumes that each actuator adds some constant value, similar to the previous model, and that it also adds some portion of the current angle. A multiplication and shift are therefore found for each actuator, and these multiplications and shifts successively applied, starting with the initial angles, to find the final angular position. While the linear model with measured values for the actuator contributions predicted the data poorly, the linear model with the least squares fitted values performed much better. The iterative model initially produced large errors, but these errors were found to be readily correctable and once removed, the iterative model predicted the data better than the linear model.

Thesis Supervisor: Steven Dubowsky
Title: Professor of Mechanical Engineering

Acknowledgments

Above all else, I would like to thank Amy Bilton for her constant help throughout this project. Her patience and experience have been invaluable. I would also like to thank Francesco Mazzini for sharing equipment and lending a hand even as he finished and prepared to defend his doctoral thesis. Congratulations and best of luck.

I am also extremely grateful to my thesis supervisor, Professor Steven Dubowsky, for the opportunity to work in the Field and Space Robotics Laboratory. I have had a great experience and learned from every minute of it.

TABLE OF CONTENTS

Figures

Tables

Chapter 1: Introduction

1.1 Background

The performance of solar concentrator systems depends on precisely shaped mirrors. However, several factors make it difficult to maintain the surface shape required for optimal performance, decreasing the effectiveness and increasing the cost of robust solar concentrators. Manufacturing high precision surfaces is both difficult and expensive. These surfaces are then subjected to thermal gradients, wind, and other disturbances that cause warping and degradation of performance [1, 2]. This project explores the use of binary actuators to adjust mirror shape in response to such disturbances, thus easing the manufacturing requirements and creating a more robust and effective system.

Though continuous actuators have been used to control surfaces [3-6], these actuators have poor reliability and are needed in large quantities with feedback sensors. Binary actuators are simpler and less expensive than continuous actuators, and offer the additional advantage of being energy efficient and lightweight. For this project, several binary actuators and elastic elements are used to control the mirror structure shown in Figure 1.1. By deploying the actuators appropriately, the shape can be adjusted with high precision through elastic averaging effects.

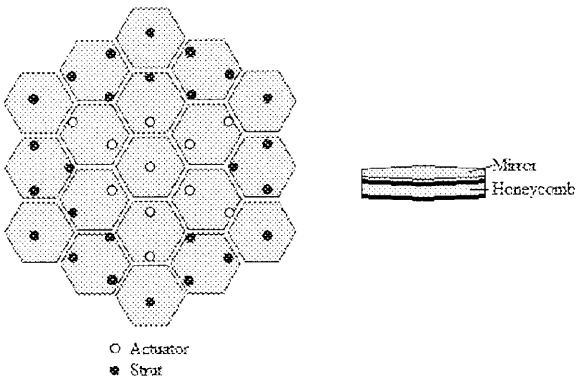

Figure 1.1: Mirror structure (modified from [1]) with cross-section of hexagon

1.2 Previous Work

In 2010, the work of Seung J. Lee investigated the use of binary actuators coupled with elastic elements to correct structural deformations. [7] Additional work published with Amy M. Bilton [1] further investigated this concept with the experiments described below.

The surface depicted in Figure 1.1 was built to demonstrate the workspace range of a binary actuated solar concentrator system. These mirrors were incorporated into the experimental system shown in Figure 1.2 and used to experimentally measure the rotational workspace of the center mirror. A honeycomb structure supports the nineteen hexagonal mirrors through thirteen actuators and thirty compliant struts.

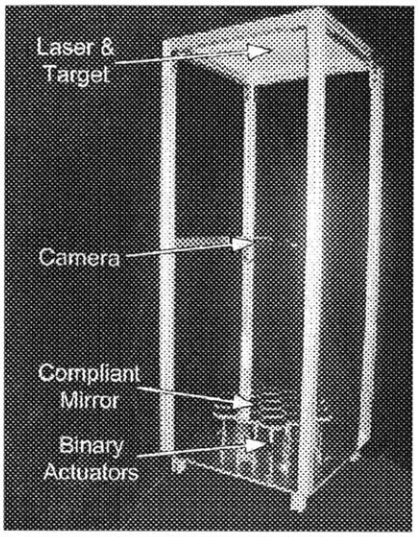

Figure 1.2: Experimental setup by Lee and Bilton [1]

Since the system uses thirteen vertical binary actuators to control the mirrors, there are 2^{13}, or 8192, possible mirror configurations. Though clustered around only nineteen distinct configurations when the compliant struts have identical stiffness, this set of solutions was distributed more evenly by randomizing the elastic element stiffness within a certain range. The dramatic improvement that was achieved can be seen in Figure 1.3. The measurements were taken with a vision-based system that reflected a laser beam off the center mirror onto a focal plane, captured images of the reflected ray with a CCD camera, and processed the images to determine the position of the reflected ray and the angular deflection of the center mirror.

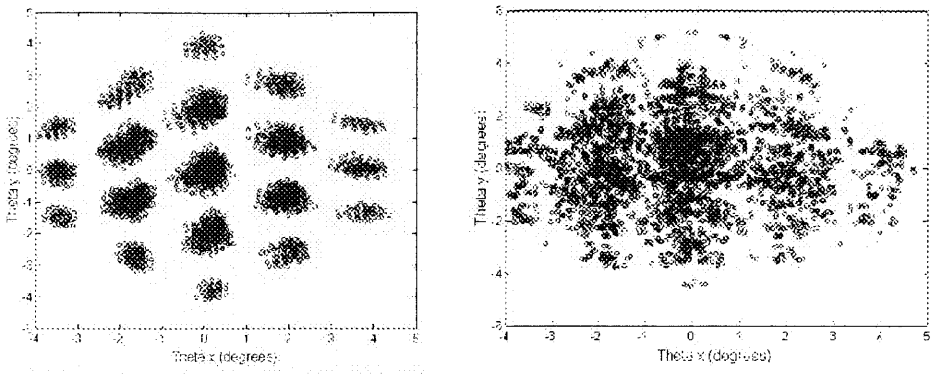

Figure 1.3: Experimentally determined rotational workspace of center mirror with identical (left) and random (right) elastic element stiffness [1]

The results were compared to the solutions calculated using the principle of superposition. The errors in the superposition solution were found to be larger than expected, which was attributed to the non-uniformity of the honeycomb structure supporting the mirrors, inaccuracies of the measurement system, and the fact that the actuators were not true binary actuators with consistent displacements due to force requirements. The percentage error increased exponentially as actuator displacement increased, as the graph in Figure 1.4 depicts. This trend was also seen in the previously calculated analysis of one and two dimensional systems; error was acceptably small for small displacements but grew exponentially with actuator stroke length.

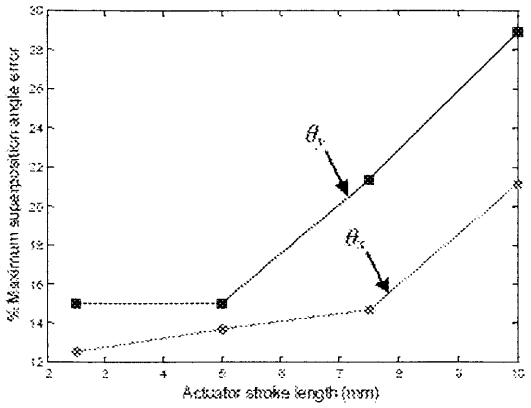

Figure 1.4: Error in center mirror angle calculation using superposition [1]

1.3 Problem Statement

The objective of this thesis is to further explore the capabilities of binary actuated mirror structures. The main focus is to develop experimentally validated models to describe the performance of the structures that can be used for control purposes. Since the experimental system has been heavily used, it must first be refurbished. In addition, software tools must be rewritten for post-processing the acquired images.

The models developed in this thesis predict the angular position of the center mirror given the actuator configuration. Two different methods are used to model and predict the system. The first model is linear and assumes that each actuator contributes the angular position of the center mirror independently of the actuator configuration; each actuator always contributes the same amount. The second model is iterative. The contribution of each actuator is dependent on the current angular position, and this dependence is modeled so that the effect of deploying each actuator is known. Starting with the initial angular position, the effect of each actuator in the configuration is

successively applied to simulate deploying the relevant actuators one by one.

Both of these models are developed and tested with data obtained by shining a laser onto the center of the mirror structure and calculating the deflection of the laser. As the actuators deploy in every possible configuration, the deflection of the laser is used to determine the corresponding angular positions. The data values are then split between calculating model parameters and testing predictions, and the models are corrected to be as accurate as possible.

1.4 Thesis Organization

This thesis is organized in four chapters. The first chapter provides the context and motivation for this research and includes the background, previous work, and problem statement. The second chapter describes the experimental setup used, including hardware, software, and data processing. Chapter 3 presents the results and models obtained, and the fourth chapter summarizes the work and suggests future experiments.

Chapter 2: Experimental Setup

2.1 Hardware Description

Figure 2.1 depicts the experimental system. An array of mirrors is mounted on a base plate, described in Section 2.1.1, which was newly constructed for this thesis. Several actuators and supporting struts attach the base plate to a larger supporting structure. A laser shines onto the center mirror through a small hole in the top panel of

this structure, and a camera is positioned to photograph the reflected laser point on the underside of the top panel.

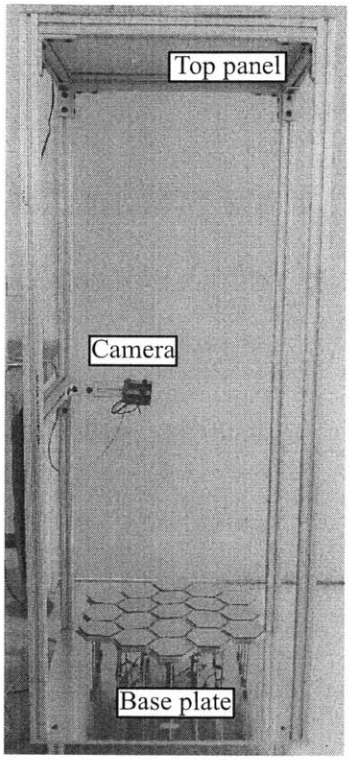

Figure 2.1: Experimental structure

Table 2.1: System parameters

Number of actuators	11
Stroke length	5 mm
Laser to mirror distance	1.354 m
Elastic element stiffness (maximum)	2000 N/m
Base plate diameter	480 mm
Base plate thickness	16 mm
Distance between camera and top panel	800 mm

2.1.1 Base Plate Description

The base plate shown in Figure 2.2 is cut to the size of the mirror array and consists of a thick honeycomb core with solid plastic top and bottom layers. The top and bottom layers of the plastic were scored with a rotary tool around the hexagons. The plastic was removed from the space between hexagons, exposing the honeycomb core between the hexagons, and a mirror was mounted on each hexagon. Large holes were drilled at the locations of the struts and actuators, and tightly fitting short pegs with threaded holes were inserted. The actuators and struts were screwed into these holes and then the base of the structure shown in Figure 2.1.

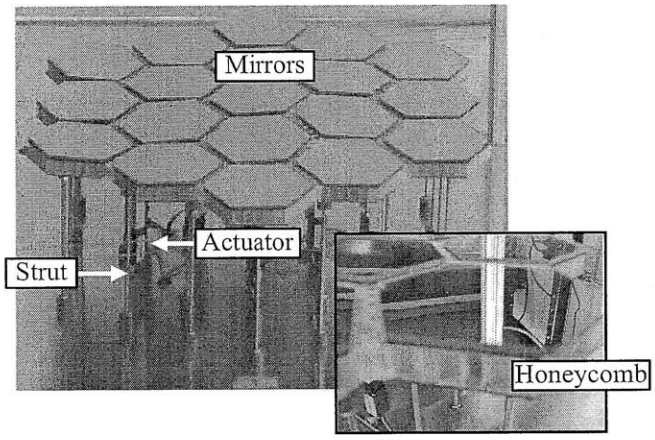

Figure 2.2: Base plate

2.1.2 Actuator and Supporting Structure Description

Eleven actuators are used in this experiment. These are programmed to extend 5 mm, and are interspersed with supporting struts. Both the actuators and supporting struts have elastic elements attached to each end, and these elastic elements screw into the base

plate or supporting structure. The stiffness of these elastic elements was randomized by punching variously sized holes through the elastic material.

The supporting structure consists of a metal frame with top and bottom panels. The metal bottom panel has threaded holes to securely attach the struts and actuators. A camera is mounted halfway up the frame, and the top panel has a small hole in the center to allow a laser mounted on top of this panel to shine down onto the mirror array.

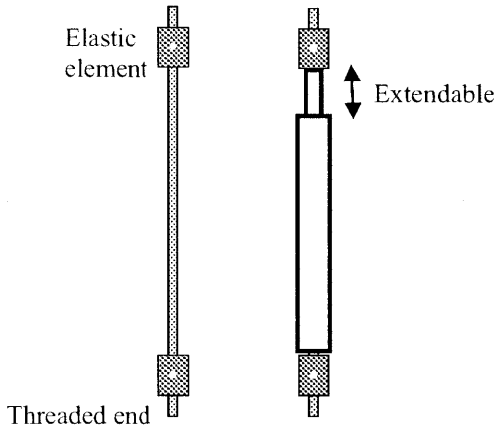

Figure 2.3: Strut (left) and actuator (right)

2.1.3 Measurement System

A red laser is directed through the hole in the top panel and onto the center mirror, which reflects the red laser point onto the top panel at a point determined by the angular deflection of the center mirror. The camera, mounted halfway up the frame of the supporting structure, is pointed upward with entire top panel in view, and records a picture for every actuator configuration. The location of the laser point in these pictures is used to determine the angular deflection of the center mirror, which is the quantity of

interest during data analysis.

2.2 Software Description

2.2.1 Experimental Software

During the experiment, the actuators are deployed to create every possible configuration. The Matlab script governing the actuators counts from zero to the possible number of configurations (two raised to the number of actuators) minus one, and converts each number to a binary number with the length equal to the number of actuators. This binary count is used to determine the series of configurations; the first digit governs the first actuator, and so on. If the digit is one, the actuator is deployed, and if the digit is zero, the actuator is not.

As each configuration is activated, the camera takes a 320 by 240 pixel, 96 dpi picture of the top panel and reflected laser point. Before these pictures are used to determine the angular deflection of the center mirror, however, some image processing is necessary for the most accurate results.

2.2.2 Post Processing

2.2.2.1 Lens Distortion Correction

Images of the reflected laser point are first corrected for camera lens distortion. As seen in the left picture of Figure 2.4, there is a severe fishbowl effect that distorts the location of the laser point. This is removed with great success using the Camera

Calibration Toolbox for Matlab® by Jean-Yves Bouguet (vision.caltech.edu/bouguetj/calib_doc), as demonstrated by the right picture of Figure 2.4.

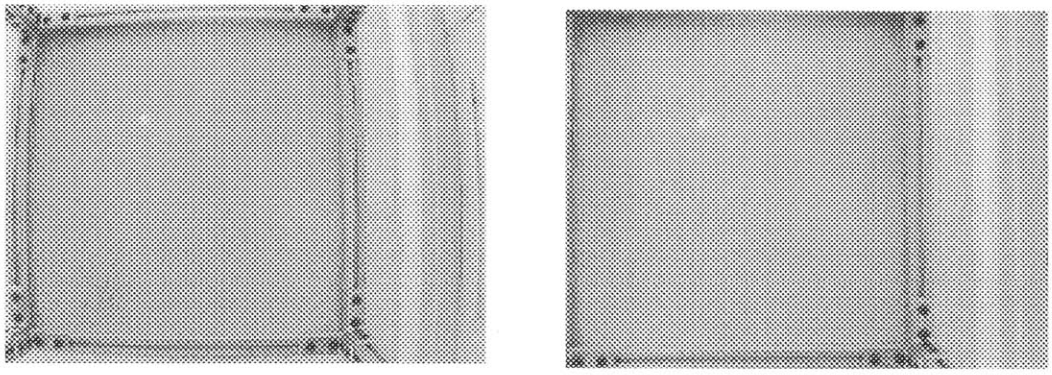

Figure 2.4: Raw image (left) and corrected image (right) of laser point

The Camera Calibration Toolbox for Matlab® requires several calibration pictures of a grid of known size, and uses a corner-finding algorithm with assistance from the user to determine the lens distortion. After a few iterations, the corners and local distortion are reprojected onto the image with great accuracy, at which point any image can be undistorted using the parameters computed by the toolbox.

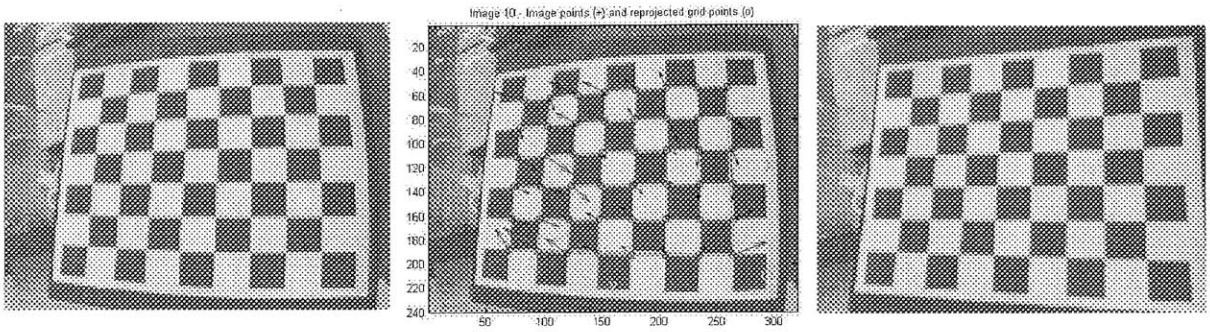

Figure 2.5: Original, reprojected, and corrected pictures for one calibration image

These parameters were computed using twenty calibration pictures similar the one shown in Figure 2.5. All contain the same image of a grid with 29 mm black and white squares, but shot from multiple heights and angles. Figure 2.6 displays the parameters that were ultimately found along with a graphical representation.

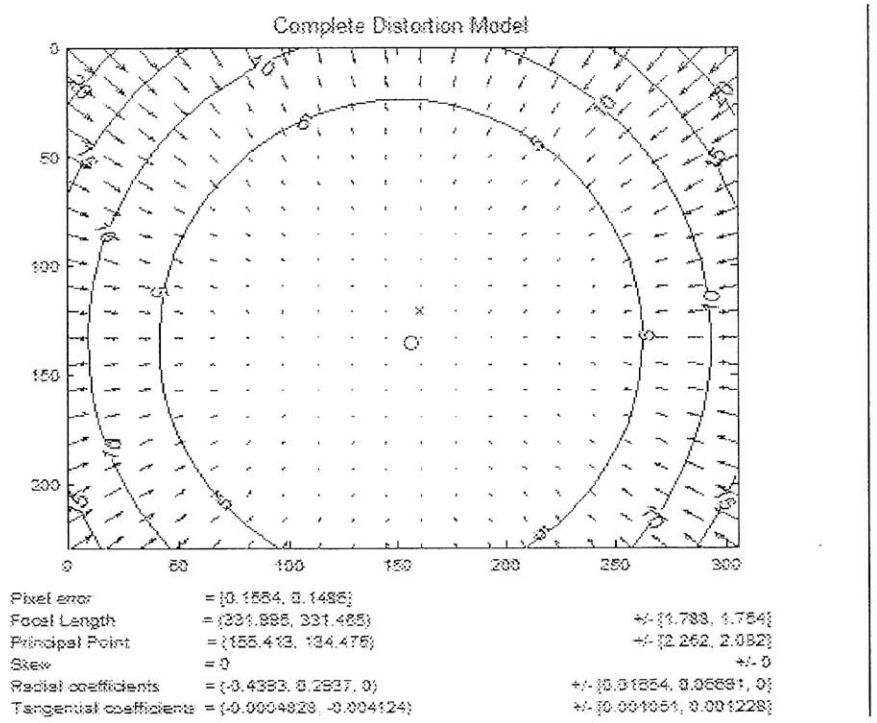

Figure 2.6: Distortion determined by calibration procedure

2.2.2.2. Reflected Ray Coordinate Calculation

After correcting the images, a Matlab script calculates the coordinates of the reflected laser point by averaging the location of the "bright" pixels. A "bright" pixel is defined as one that falls within a certain range of brightness for the red, blue, and green frames, where the ranges are different for each color and the pixel must satisfy all three. The edges of the image and a circular area encompassing the center hole, through which the laser shines, are excluded since these regions have false bright spots.

This results in the origin of the coordinate system being located in the top left corner of the image. However, the center hole of the top panel must be the origin of the coordinate system in order to simplify angle calculations. The location of the center hole is constant in each picture, since the camera never moves, and is therefore found manually. These coordinates are then used to shift the coordinates of the laser point so that the center hole is the origin of the coordinate frame.

Measurements of the structure's dimensions are compared with their size in the image to obtain a pixel-to-distance conversion ratio. This allows the hole-centered coordinates to be converted to physically measurable units, which is necessary to include the height from the top panel to the center mirror in calculations. This dimension is needed to calculate the angular position of the center mirror.

2.2.2.3 Calculation of Angles

The center mirror has two degrees of freedom. These will be described as θ_x and θ_y, as shown in Figure 2.7. The x or y component of the laser point coordinates and the

distance from the center hole to the mirror (L) form two legs of a right triangle,[1] so that the calculated values of θ_x or θ_y are defined as follows.

$$\hat{\theta}_x = \tan^{-1}(x/L)$$
$$\hat{\theta}_y = \tan^{-1}(y/L) \qquad [2.1]$$

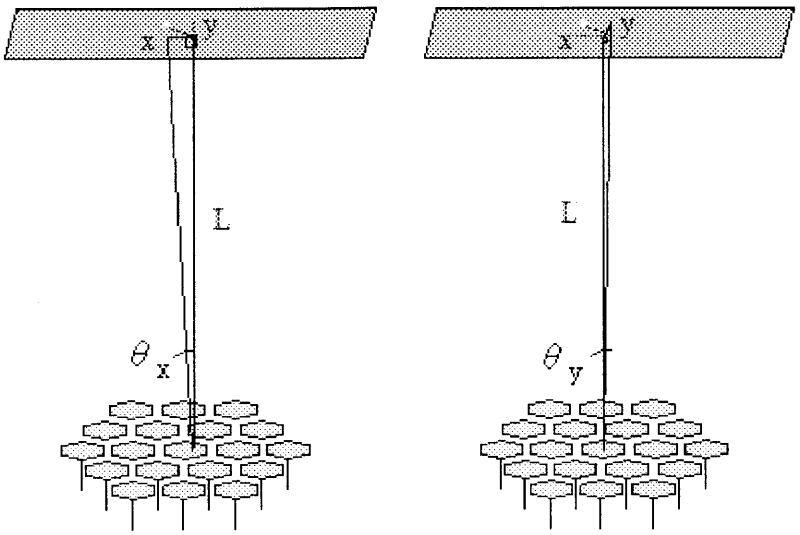

Figure 2.7: Diagram of θ_x and θ_y

These calculations therefore result in two angles for every actuator configuration, after correcting the images of the top panel for lens distortion and extracting the coordinates of the reflected laser point relative to the center hole. These angles are the data that will be examined from this point forward.

1 The laser is assumed to be completely vertical

Chapter 3: Experimental Results

3.1 Experiment Description

The eleven actuators allowed 2^{11}, or 2048, unique actuator configurations. A picture was taken of the reflected laser point for each one and the corresponding angular configurations were calculated as previously described. Each actuator had a stroke length of 5 mm and an elastic element on each end. These elastic elements had random stiffness as described in Section 2.1.2 and contributed varying amounts to the length of the actuator.

Figure 3.1 shows every set of angles obtained. Since the effect of each actuator on the final angles is desired, this plot will be broken down by actuator and angle to determine what relationships exist and whether they are able to predict the angles of the center mirror given only the actuator configuration.

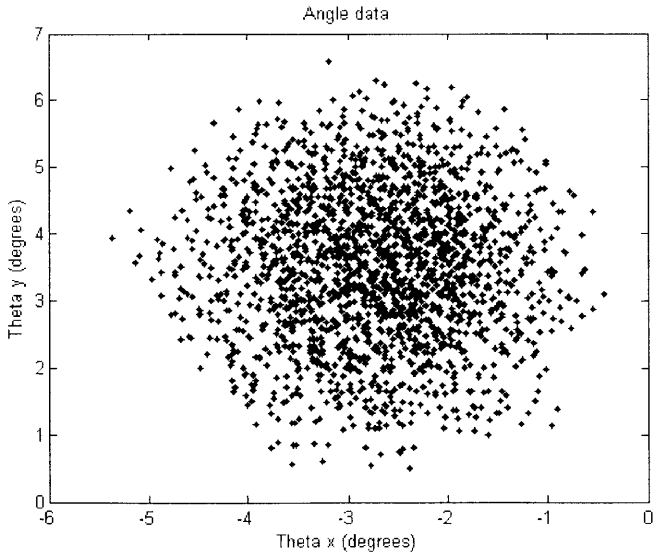

Figure 3.1: Complete data set

3.2 Model Descriptions

An accurate system model would allow the final angles to be calculated from only the actuator configuration, allowing useful predictions and facilitating analysis of the system and its workspace. Two different models are formed and tested against the experimental data. The first is a linear model that sums the contributions of each actuator, which are assumed to not vary. These contributions are found by two different methods and the results compared. The second model is iterative; each actuator is assumed to add a fraction of the current angle in addition to a constant contribution. The effect of each actuator in the configuration is successively applied, starting with the initial angles, to find the angular position.

3.3 Linear Model

3.3.1 Model Description

For the linear model, each actuator is assumed to always contribute the same amount to the final angle. The angles can therefore be calculated as:

$$\hat{\theta} = A\,u$$

$$\begin{bmatrix} \hat{\theta}_x \\ \hat{\theta}_y \end{bmatrix} = \begin{bmatrix} a_{x1} & a_{x2} & \cdots & a_{xn} \\ a_{y1} & a_{y2} & \cdots & a_{yn} \end{bmatrix} \begin{bmatrix} u_1 \\ u_2 \\ \vdots \\ u_n \end{bmatrix} \qquad [3.1]$$

where n represents the number of actuators and u is a vector of zeros and ones indicating which actuators are deployed. If the first entry is a one, the first actuator is deployed, and

so on. The coefficient a_{xi} is the contribution of actuator i to θ_x, and a_{yi} is the contribution to θ_y. By multiplying the actuator and coefficient matrices, the contributions to each angle by the deployed actuators are summed.

3.3.2 Parameter Identification

Two different methods were used to identify the system coefficient matrix for the linear model. These methods, described below, include directly measuring the individual actuator contributions and least squares fitting of a large data set.

3.3.2.1 Measured Values

It is assumed that if each actuator always contributes the same amount to the final angle, then the values for each actuator should be the change in angle obtained when only that actuator is deployed. The coefficients a_{xi} and a_{yi} are therefore the experimental θ_x and θ_y values obtained when only actuator i is deployed.

3.3.2.2 Least squares method

In an alternative method for determining the system matrix shown in Equation 3.1, a least squares method is used to find optimal values for a_{xi} and a_{yi}. While the underlying assumption remains that each actuator contributes to the angles independently of the configuration, obtaining the best fitting a_{xi} and a_{yi} values allows some flexibility. When using least squares, these parameters are chosen to smooth out whatever deviations exist in each actuator's contributions to the angles.

A subset of the measurements are used to determine the least squares fitting. Equation 3.1 can be extended to represent the m measurements used for the fitting, obtaining Equation 3.2

$$\begin{bmatrix}\theta_1 & \theta_2 & \cdots & \theta_m\end{bmatrix} = A\begin{bmatrix}u_1 & u_2 & \cdots & u_m\end{bmatrix} \qquad [3.2]$$

where A is the system matrix, θ_i represents the ith experimental angular data, and u_i represents the ith input vector of zeros and ones.

The ordinary least squares solution to $\theta = Au$ is found using Matlab so that A minimizes the sum of squared errors $(\theta - Au)'(\theta - Au)$. The number of data points used in the least square fitting, m, is approximately half of the total data taken. The coefficients found using the least squares fitting are shown in Appendix A. The effectiveness of this method is evaluated by comparing the predicted results to the experimental data below.

3.3.2.3 Treatment of Initial Angles

For the linear model, the initial angles were subtracted from the angular data before determining the system matrix. Therefore, the a_{xi} and a_{yi} measured values are actually the θ_x and θ_y values obtained when only actuator i is deployed minus the initial angles, and the angular matrix θ used to calculate the least squares fitting consists of the experimentally found angles minus the initial angles. The initial angles are added to the linear model predictions before comparing them to the experimental data.

3.4 Iterative Model

While processing the data, a the effect of each actuator was analyzed by plotting all of the data with the actuator on and all the data with the actuator off as shown in Figure 3.2. During this analysis, a consistent shift in the angular data is revealed. Such a consistent shift indicates that given any starting angles, the angles after deploying the actuator could be predicted with reasonable accuracy.

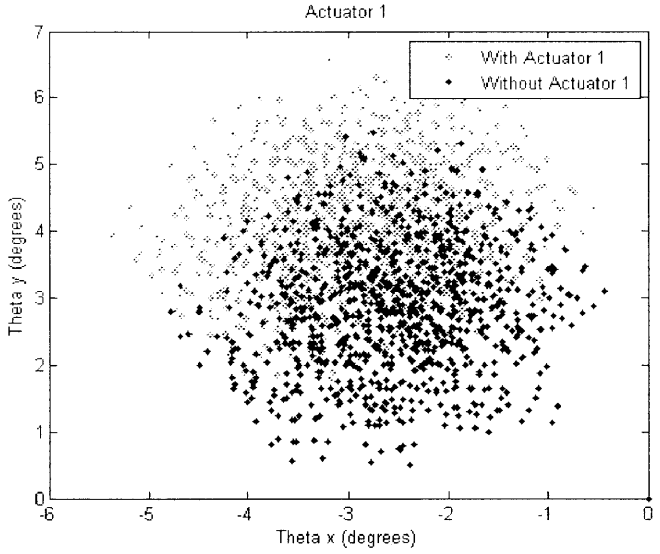

Figure 3.2: Shift in data when actuator is on versus off

This consistent shift motivates the iterative model described here. In this model, the angular effect of each actuator that is deployed is successively applied to determine the final mirror angle. It is assumed that there is a one-to-one relationship between the angle before the actuator is turned on (θ^{k-1}) and afterward (θ^{k}) as shown:

$$\theta^{k} = f(\theta^{k-1}) \qquad [3.3]$$

For this approach, the function that defines the relationship between the angles must be determined. Figure 3.3 plots the x-angle with and without an actuator, and Figure 3.4 plots the y-angle. The plots reveal a clearly linear relationship between the angles obtained when the actuator is deployed and the angles obtained when the actuator is not. When similar plots are made for the other actuators, it becomes clear that each actuator has a linear trend. The remainder of the actuator trend plots are shown in Appendix A. Though some actuators have a cleaner relationship than others, the trend is very good after the first few actuators.

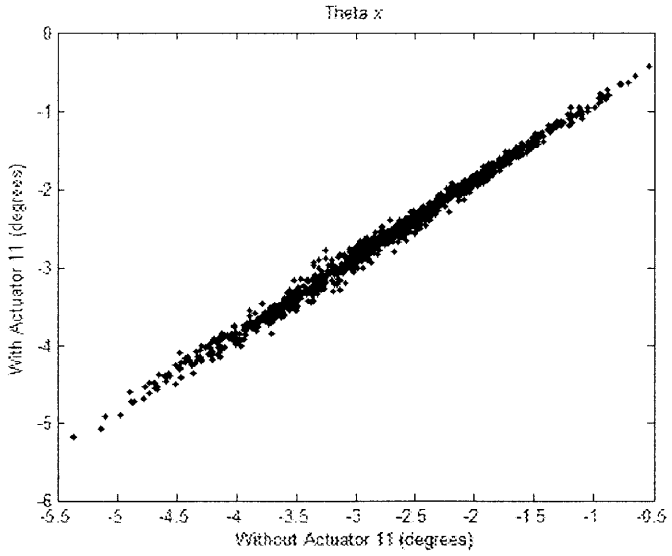

Figure 3.3: θ_x with and without actuator

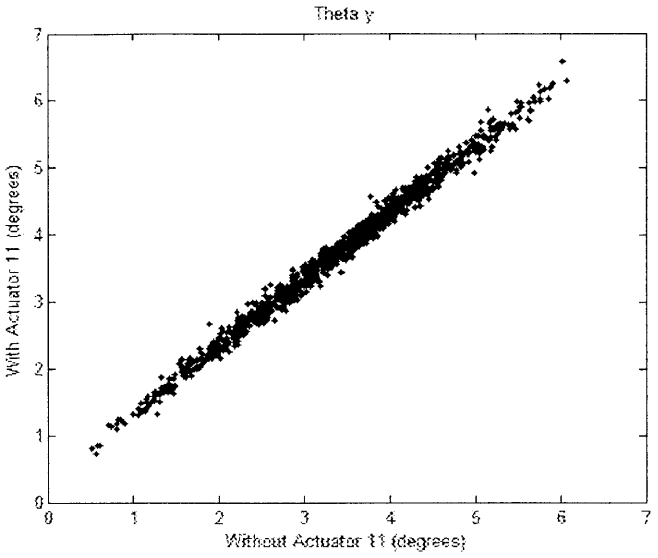

Figure 3.4: θ_y with and without actuator

A least squares linear fit for each plot is obtained from 1000 randomly chosen data values and incorporated into the iterative model. The fit obtained for each line consists of a slope and intercept, referred to as a multiplication and shift from now on.

In this iterative model, each actuator configuration is simulated by first applying the multiplication and shift for the first actuator in that configuration to the initial angle, then successively applying the multiplication and shift for the next actuator to the preceding result until the entire configuration is simulated. Equation 3.4 shows the mathematical representation of this method where θ_{x0} and θ_{y0} represent the initial angles and m_i and b_i represent the multiplication and shift for actuator i. Every line incorporates another actuator into the angle calculation.

$$\begin{aligned}\hat{\theta}_x &= m_1\theta_{x0}+b_1 \\ &= m_2(m_1\theta_{x0}+b_1)+b_2 \\ &= m_3(m_2(m_1\theta_{x0}+b_1)+b_2)+b_3 \\ &\ldots \\ &= m_i(\ldots(m_2(m_1\theta_{x0}+b_1)+b_2)\ldots)+b_i\end{aligned} \qquad [3.4]$$

Similarly,

$$\hat{\theta}_y = m_i(\ldots(m_2(m_1\theta_{y0}+b_1)+b_2)\ldots)+b_i \qquad [3.5]$$

It is worth noting that while Equations 3.4 and 3.5 seem to imply that all actuators are included, only those that are deployed in the configuration are part of these equations. The parameters m_i and b_i are absent from the calculations or set to 1 and 0, respectively, when actuator i is not deployed.

Additionally, while m_i and b_i are used in both Equations 3.4 and 3.5 for clarity, these parameters differ for θ_x and θ_y. Each actuator therefore has four fit parameters associated with it, most accurately represented as m_x, b_x, m_y, and b_y. The experimentally determined parameters are shown in Appendix A. Approximately half of the data values are used to find this fit. The rest are set aside so that predictions calculated using this method can be compared to the experimental results.

3.5 Model Results

3.5.1 Linear Model: Measured Values

Predicted angles using the linear model with the coefficients determined using measured values are plotted against the experimental results in Figure 3.5. As can be seen in this plot and Figure 3.6, which shows the percent error for θ_x and θ_y, the predictions are very poor. Therefore, this model will only be explored with A calculated by the least squares method.

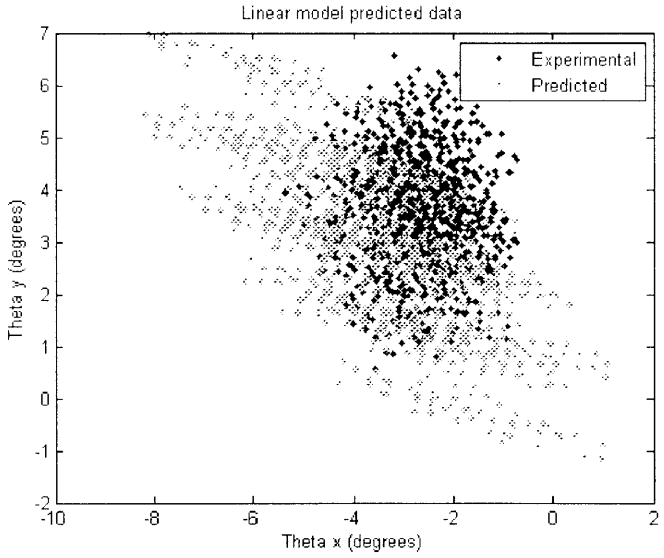

Figure 3.5: Prediction results for linear model with measured values

The error is defined as

$$E_\theta = \hat{\theta} - \theta \qquad [3.6]$$

where $\hat{\theta}$ is the predicted angular data and θ is the experimental data.

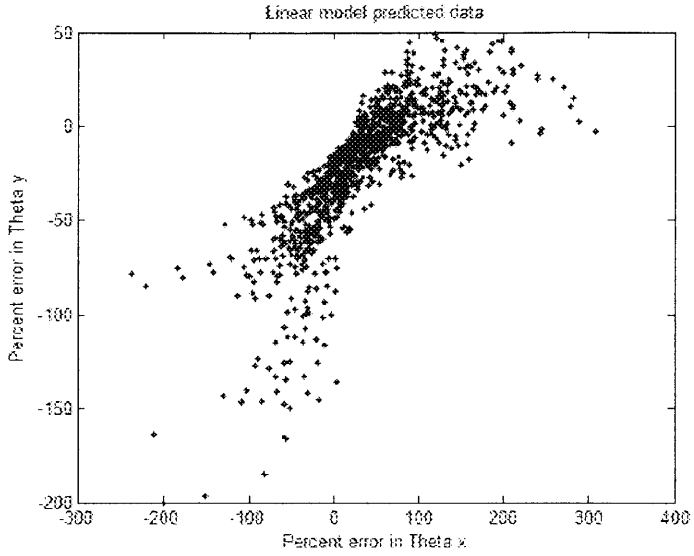

Figure 3.6: Percent error for linear model with measured values

3.5.2 Linear Model: Least Squares Method

A randomly selected portion of the data was used to determine the coefficients for the linear model using a least squares fit. The remainder of the data and the linear model predicted values are shown in Figure 3.7. The predicted values are slightly skewed from the experimental data along one direction, potentially indicating a problem with an individual actuator.

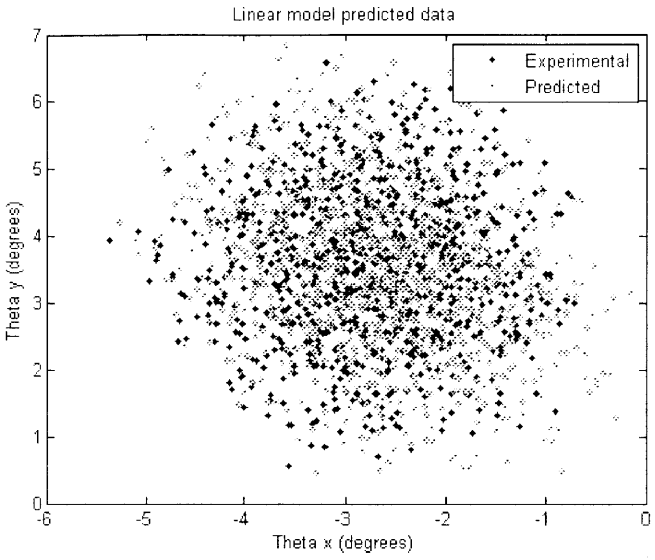

Figure 3.7: Prediction results for linear model with least squares values

Figure 3.8 plots the percent error in θ_x and θ_y, revealing errors commonly up to 40% for θ_x and 20% for θ_y, with some error values much greater.

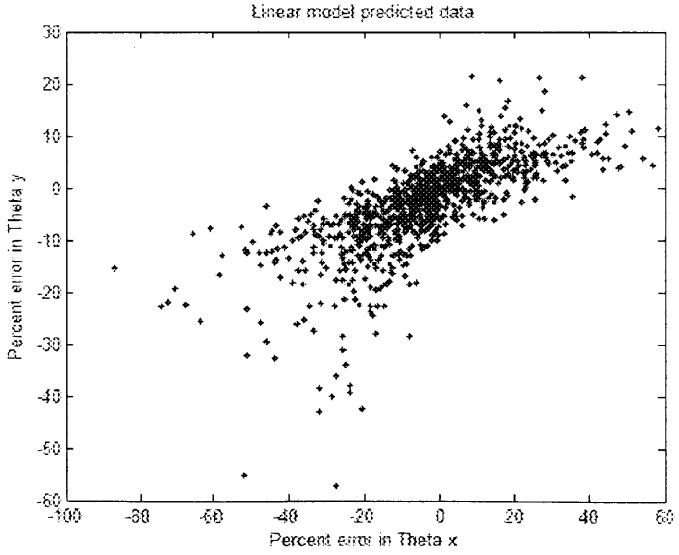

Figure 3.8: Percent error for linear model with least squares values

3.5.3 Iterative Model

Figure 3.9 shows the experimental data values that were not used to calculate the iterative model and the corresponding predicted values. Significant errors appear, but these appear to be readily correctable since the error is mostly a shift.

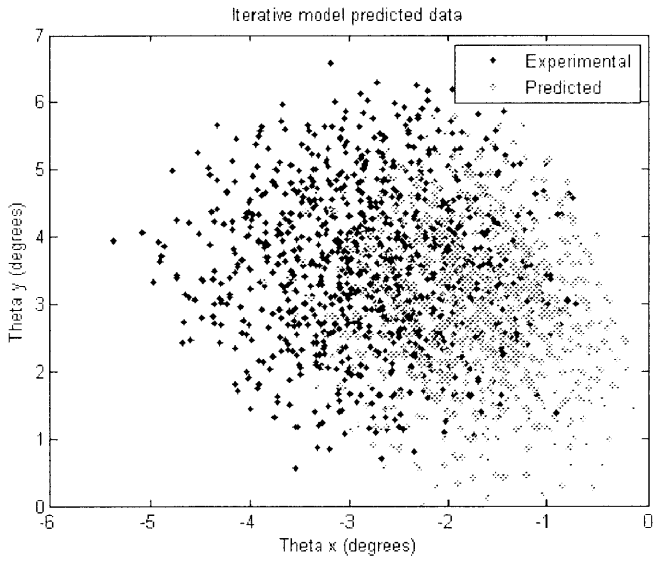

Figure 3.9: Prediction results for iterative model

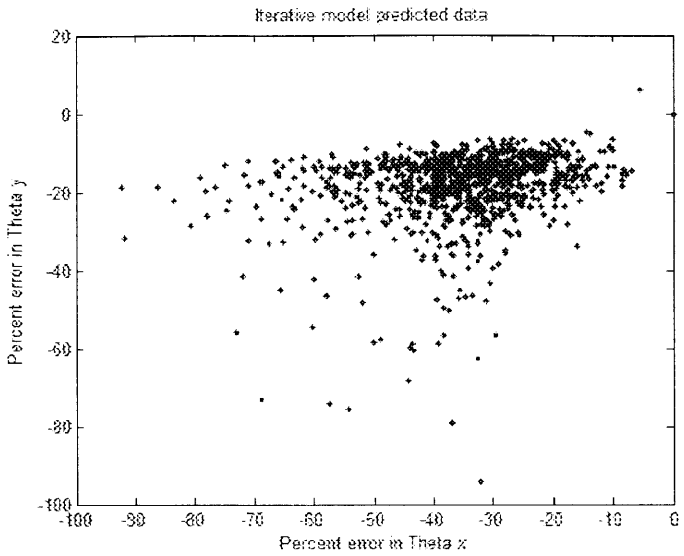

Figure 3.10: Iterative model percent error

Figure 3.10 displays the percent error in both θ_x and θ_y. The percent error is up to 60% for θ_x and 30% for θ_y, with many errors much larger. To adjust the model and reduce this error, Figures 3.11 and 3.12 plot the predicted and experimental θ_x and θ_y values against each other. As Figure 3.9 suggests, the error is largely predictable.

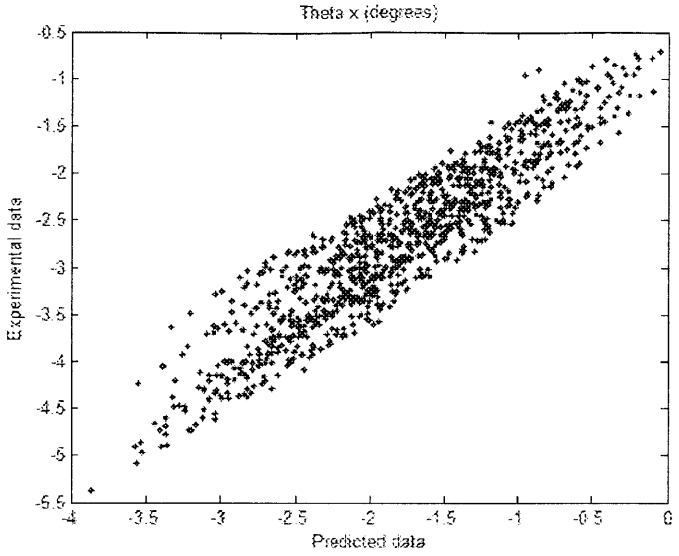

Figure 3.11: Iterative model predictions versus experimental values of θ_x

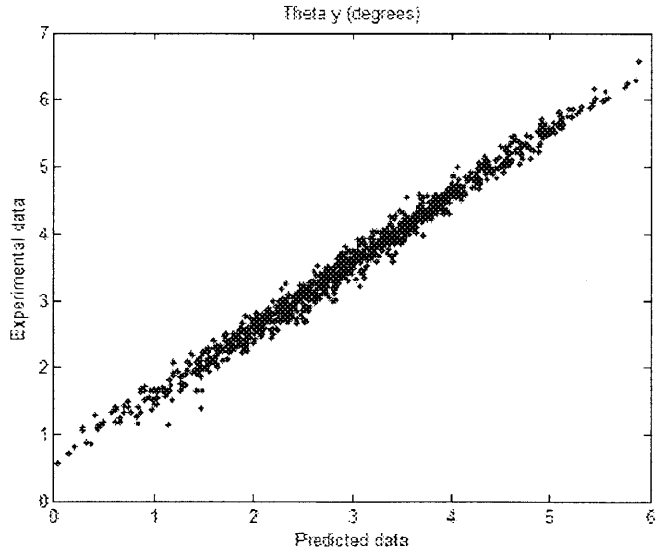

Figure 3.12: Iterative model predictions versus experimental values of θ_y

These relationships are roughly linear. Figures 3.11 and 3.12 are recreated with the data values initially used to calculate the model parameters, and the linear fit for these

plots is then calculated with Matlab. The slope and intercept of these linear fits, M_x, B_x, M_y, and B_y, indicate that the error is essentially a pure shift for each angle since the multiplicative coefficients M_x and especially M_y are close to 1. These will still be used as they do allow a slight improvement to the model, particularly when predicting θ_x. All fit values can be viewed in Appendix A.

The predictions are then multiplied and shifted by these values, and replotted against the experimental values in Figure 3.13.

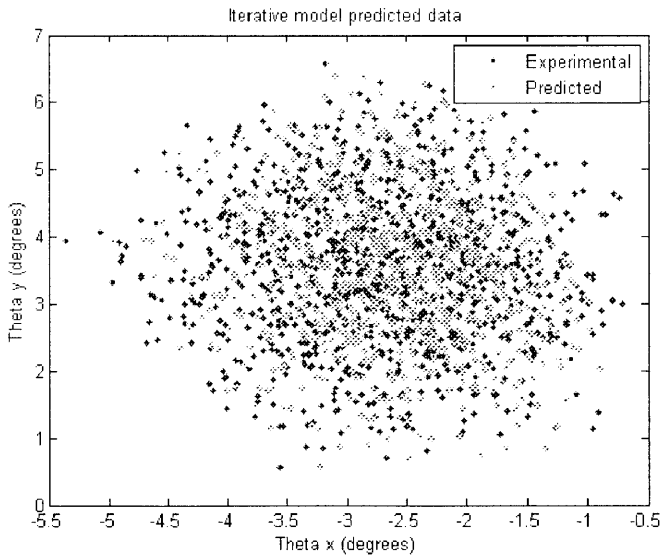

Figure 3.13: Prediction results for corrected iterative model

The agreement is much better, and the percentage error plotted in Figure 3.13 confirms that the error is greatly reduced. Percent error is now mostly under 25% for θ_x and 10% for θ_y, with some errors still much larger.

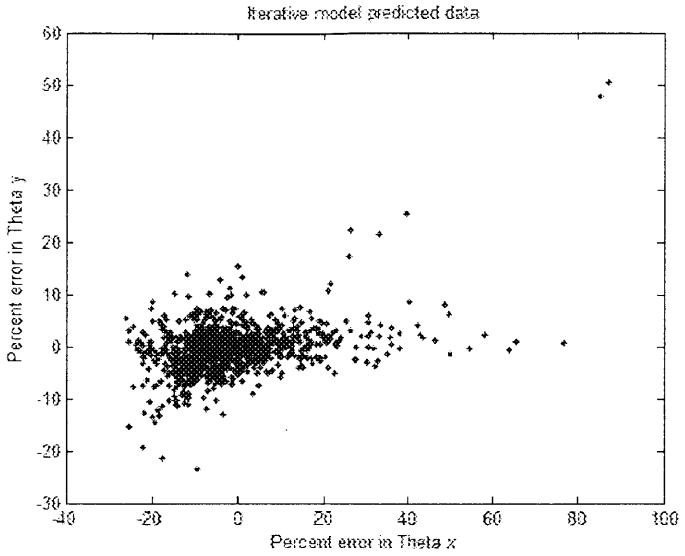

Figure 3.14: Percent error for corrected iterative model

Chapter 4: Summary and Conclusions

4.1 Conclusions

This project uses binary actuators to adjust the shape of a mirror structure. It explores the contribution of each actuator to the angular position of the center mirror, with the goal of modeling the angular position given the actuator configuration. The angles are calculated using the location of a laser point reflected off the center mirror for all possible actuator configurations, and these values are used to make, test, and correct models for the angular position.

Two models were explored: a linear model that assumes each actuator's contribution is independent of the configuration, and an iterative model that successively

applies a multiplication and shift for each actuator. The iterative model had significant errors, but these were largely corrected by finding a linear fit between the predicted and experimental data, then applying that multiplication and shift to each angle. The corrected iterative model proved to be more accurate than the linear model, though least squares values for the actuator contributions greatly improved the latter.

The higher error values in both models could be attributed to faulty actuators, non-uniform actuator stroke length, irregularities in the base plate, and tilt in the laser, among other factors.

4.2 Suggestions for Future Work

Both models could likely be improved by eliminating the initial angle and using a shorter actuator displacement. In addition, constructing the base plate core from a more uniform material might reduce the errors and allow accurate models to be calculated from basic material properties. Stiffer elastic elements could make the contribution from each actuator more predictable, though this may have other undesirable effects on the system such as clumping the possible angles or reducing the actuator stroke length that could damage the base plate.

It is therefore suggested that future work use shorter displacements and reduce the initial angle, and that the softest elastic elements are replaced with stiffer ones to make the actuator contribution more predictable.

References

1. Lee, S. J., Bilton, A. M., and Dubowsky, S., 2010, "On the Kinematics of Solar Mirrors Using Massively Parallel Binary Actuation." ASME DETC2010-28875.
2. Coventry, J. S., 2005, "Performance of a Concentrating Photovoltaic/Thermal Solar Collector," Solar Energy, **78**, pp. 211-222.
3. Gardner, J. P. et al, 2006, "The James Webb Space Telescope." Space Science Reviews, **123**(4), pp. 485-606.
4. Burge, J. H., Baiocchi, D., Cuerden, B., 2001, "Ultralight Active Mirror Technology at the University of Arizona." Optomechanical Engineering 2000, Proc. Of SPIE, **4198**.
5. Irschik, H., 2002, "A Review on Static and Dynamic Shape Control of Structures by Piezoelectric Actuation." Engineering Structures, **24**, pp. 5-11.
6. Crawley, E. F., 1994, "Intelligent Structures for Aerospace: A Technology Overview and Assessment." AIAA Journal, **32**(8), pp. 1689-1699.
7. Lee, S.J., 2010, "Planar Feasibility Study for Primary Mirror Control of Large Imaging Space Systems Using Binary Actuators." M.S. Thesis, Massachusetts Institute of Technology, Cambridge, MA.

Appendix A

A.1 Linear model

A.1.1 Measured Values

Table A.1: Measured values for a_{xi} and a_{yi} in degrees

Actuator	a_{xi}	a_{yi}
1	-1.8587	1.9531
2	-0.7131	1.3896
3	-0.9608	0.2224
4	-1.6684	0.2792
5	-1.7691	0.7427
6	-1.1144	1.3583
7	0.0851	1.5530
8	-0.3104	0.0196
9	-0.5560	0.1815
10	-0.2468	0.1834
11	0.0473	0.2495

A.1.2 Least Squares Method

Table A.2: Least squares values for a_{xi} and a_{yi} in degrees

Actuator	a_{xi}	a_{yi}
1	-0.7134	1.5732
2	0.3444	1.0317
3	0.0253	-0.2883
4	-0.9734	-0.2251
5	-1.2263	0.4375
6	-0.9463	1.2122
7	0.1243	1.3792
8	-0.2361	0.0238
9	-0.7146	0.3312
10	-0.4971	0.5704
11	-0.2716	0.6586

A.2 Iterative Model

A.2.1 Remaining actuator plots

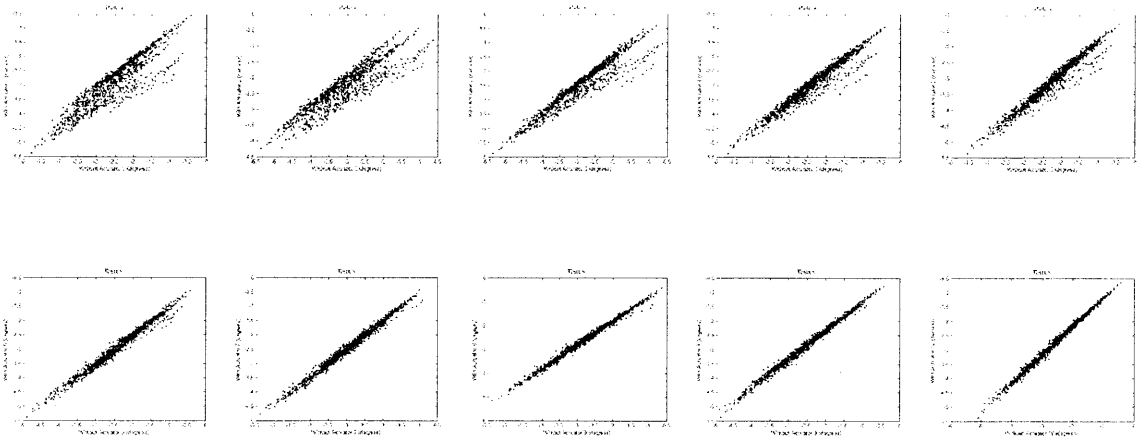

Figure A.1: θ_x for the remaining actuators

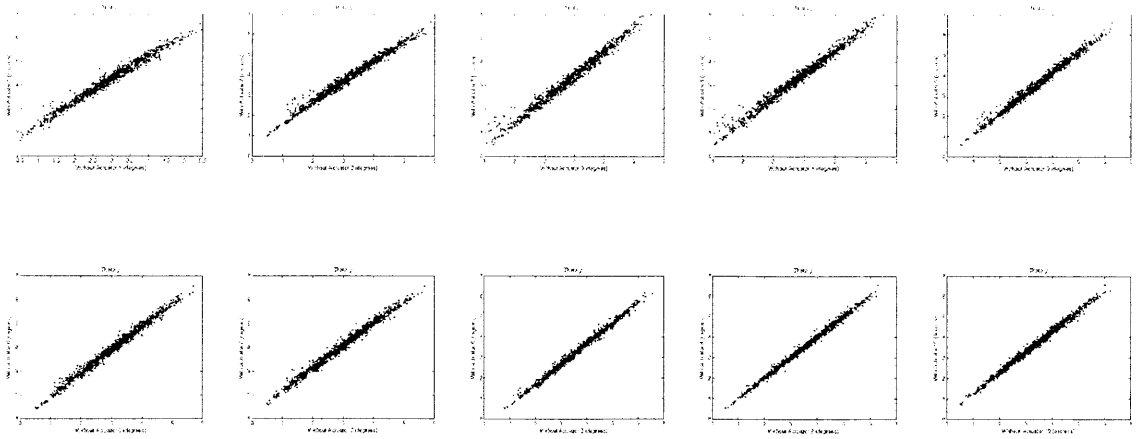

Figure A.2: θ_y for the remaining actuators

A.2.2 Iterative model parameters

Table A.3: Iterative model parameters
Note that m is dimensionless and b has units of degrees

Actuator	m_x	b_x	m_y	b_y
1	0.9972	-0.3647	0.9457	1.4263
2	0.7573	0.0195	0.9877	0.7143
3	0.9185	0.1681	0.9864	-0.5498
4	0.9823	-0.6467	0.9687	-0.4028
5	0.9574	-0.9705	0.9867	0.1739
6	0.9773	-0.5985	0.9721	0.9751
7	0.9798	0.4311	0.9403	1.2540
8	0.9994	0.1696	0.9923	-0.2882
9	1.0032	-0.3279	1.0062	-0.0015
10	0.9945	-0.1869	1.0046	0.2847
11	0.9875	0.0840	1.0020	0.3338

Table A.4: Iterative model corrective parameters
M_x and M_y are dimensionless, B_x and B_y have units of degrees

M_x	B_x	M_y	B_y
1.0942	-0.7421	1.0061	0.5679